Unified model of tectonics and heat transport in a frigid Enceladus

Gustavo Gioia*, Pinaki Chakraborty†, Stephen Marshak†, and Susan W. Kieffer†‡

Departments of *Mechanical Science and Engineering and †Geology, University of Illinois at Urbana–Champaign, Urbana, IL 61801

Contributed by Susan W. Kieffer, June 26, 2007 (sent for review May 16, 2007)

Recent data from the Cassini spacecraft have revealed that Enceladus, the 500-km-diameter moon of Saturn, has a southern hemisphere with a distinct arrangement of tectonic features, intense heat flux, and geyser-like plumes. How did the tectonic features form? How is the heat transported from depth? To address these questions, we formulate a simple model that couples the mechanics and thermodynamics of Enceladus and gives a unified explanation of the salient tectonic features, the plumes, and the transport of heat from a source at a depth of tens of kilometers to the surface. Our findings imply that tiny, icy moons can develop complex surficial geomorphologies, high heat fluxes, and geyser-like activity even if they do not have hot, liquid, and/or convecting interiors.

Enceladus, the 500-km-diameter moon of Saturn, is the smallest body in the solar system with erupting plumes (1). On the southern hemisphere, Enceladus displays tectonic features that are closely related to the plumes, a thermal anomaly that straddles the south pole, and high rates of heat flow in coincidence with the thermal anomaly (2, 3). The tectonic features include four 130-km-long fractures that cut across the thermal anomaly and are known as "tiger stripes" (2, §). The plumes observed by Cassini gushed from vents located on the tiger stripes (5); these plumes had a total discharge similar to the Old Faithful geyser in Yellowstone National Park and consisted of H_2O, CH_4, N_2, and CO_2 gases laden with ice crystals (1, 2, 6).

The cause of plume eruption has been addressed by two antithetic models so far. In one model, called "Cold Faithful," Enceladus has a shell of H_2O ice with pockets of liquid water at depths as shallow as 7 m (2). Cold Faithful's plumes erupt where small fractures decompress the pockets of liquid water, causing the liquid water to boil at a temperature of at least 273 K. The small fractures may form (and the attendant plumes erupt) at any time, driven by tectonic disturbances. Thus, the plumes of Cold Faithful may remain active over long periods of time.

In the other model, called "Frigid Faithful," Enceladus has a shell of H_2O ice and H_2O clathrates (CO_2, CH_4, N_2) topped with a layer of H_2O–CO_2 ice (Fig. 1) (7). Frigid Faithful is based on the assumption that the composition of the plumes observed by Cassini indicates the composition of the shell where the plumes originate. The plumes of Frigid Faithful erupt where large fractures (the tiger stripes) expose and decompress some clathrates of the clathrate-rich shell, causing these clathrates to absorb heat from a source at depth and then to dissociate at a temperature that might be as low as ≈133 K, the average temperature of the hotspots that have been observed on the surface of the south pole (3). The tiger stripes need to form and expose some clathrates of the shell only once, possibly long ago in geologic time. Although clathrate dissociation is, in principle, self-limiting (because the products of dissociation may refreeze), it is also explosive (8). As a result, the dissociation of some clathrates exposes more clathrates, which may in turn dissociate explosively and expose even more clathrates. Thus, the plumes of Frigid Faithful may remain active over long periods of time. The gaseous products of clathrate dissociation rush up the tiger stripes, advecting heat to the surface of Enceladus, where they may occasionally leak out in the form of plumes (Fig. 1).

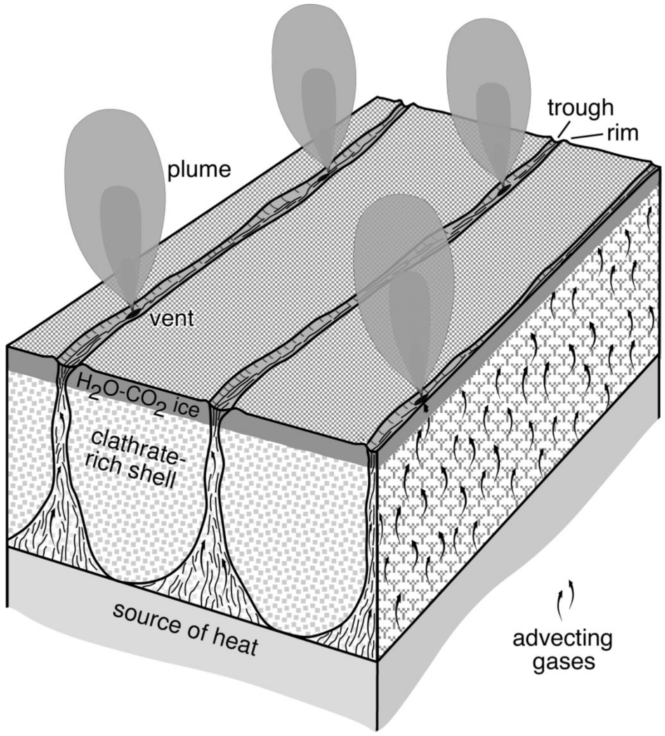

Fig. 1. Schematic of Frigid Faithful. In the text, we argue that the tiger stripes (and the advection of heat by the fast-moving, gaseous products of clathrate dissociation) extend to a depth of ≈35 km, turning the shell of Enceladus into a deep and frigid "advection machine." The plumes are but leaks in this advection machine.

The advection of heat extends to the same depth as the tiger stripes. As we shall argue below, in Frigid Faithful the tiger stripes extend to a depth of ≈35 km into the clathrate-rich shell, turning the shell into a deep "advection machine." In contrast to heat conduction, heat advection by fast-moving gases does not require large temperature gradients (9, 10), with the implication that Frigid Faithful's shell remains close to the surficial temperature up to a depth of ≈35 km. Note that the shell remains frigid precisely because it conveys heat very efficiently; as Lorenz (11) has pointed out in a discussion of active geysering on Triton, a moon of Neptune, "one must not equate a cold, low-energy environment with an absence of energetic phenomena" (such as

Author contributions: G.G., P.C., and S.W.K. designed research; G.G., P.C., S.M., and S.W.K. performed research; G.G., P.C., S.M., and S.W.K. analyzed data; and G.G. wrote the paper.

The authors declare no conflict of interest.

Abbreviation: TST, tiger-stripe terrain.

‡To whom correspondence should be addressed. E-mail: skieffer@uiuc.edu.

§Helfenstein, P., Thomas, P. C., Veverka, J., Rathbun, J., Perry, J., Turtle, E., Denk, T., Neukum, G., Roatsch, T., Wagner, R., *et al.* (2006) *Lunar Planet Inst Conf Abstr* 37:2182. Available at www.lpi.usra.edu/meetings/lpsc2006/pdf/2182.pdf.

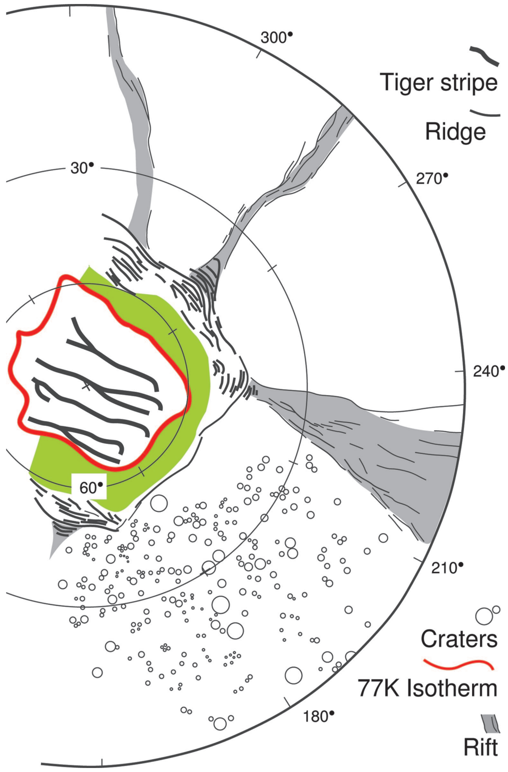

Fig. 2. Map of the major tectonic features on the southern hemisphere of Enceladus. [Based on figure 2 in Porco *et al.* (2) and *The Enceladus Atlas* (19).] The region shown in green is the annular region that surrounds the TST and contains modest topography.

heat transport). Conversely, we argue that vigorous heat transport is compatible with a frigid environment.

A frigid environment entails negligible rates of deformation by creep (12, 13), with implications for the choice of a mechanical model of Frigid Faithful's shell. In addition, H_2O clathrates are intrinsically much stiffer (in the sense of less deformable by creep) than H_2O ice, especially at low temperatures (14). In fact, Barr and McKinnon (13) have shown that an Enceladus with a clathrate-rich icy shell would be so stiff as to preclude solid-state convection in the shell. It follows that Frigid Faithful is incompatible with mechanical models that invoke solid-state convection to explain some of the tectonic features on icy moons such as Europa and Miranda (15, 16). [Note, however, that solid-state convection (13), and diapirism in particular (17), remains compatible with Cold Faithful.] In view of the negligible rates of creep to be expected in a shell that is both clathrate-rich and frigid, we model Frigid Faithful's shell as a brittle elastic body. To complete our mechanical model of the shell, we turn for guidance to a description of the terrains and tectonic features observed by Cassini on the southern hemisphere of Enceladus.

The southern hemisphere can be divided into four distinct terrains, each seemingly associated with a different stress regime (Fig. 2). (*i*) An innermost "tiger-stripe terrain" (TST) that contains the surface expression of four mutually parallel, evenly spaced ($\approx$35 km), 130-km-long fractures (2) (the tiger stripes), which we interpret as tensile fractures. The surface expression of a tiger stripe consists of a 0.5-km-deep, 2-km-wide trough (Fig. 1) with a longitudinal axis oriented 45°W (2). The TST coincides with a thermal anomaly, which we may define as the surface area enclosed by the isotherm of 77 K measured by Cassini (2) (Fig. 2). With this definition, both the thermal anomaly and the TST are approximately rectangular in shape (a fact to which we return later), with the slightly longer sides of the rectangle parallel to the surface expression of the tiger stripes. (*ii*) A narrow annular terrain (latitude $\approx$60°S) that surrounds the TST and contains modest topography and no salient tectonic features. (*iii*) A second annular terrain that contains a prominent ring of compressional ridges.§ These ridges are best developed on the parts of the ring that run approximately parallel to the tiger stripes and the longer sides of the TST. (*iv*) An outer terrain that can only be mapped with certainty in the interval from 180°W to 360°W, where it contains three tensile radial rifts§ that propagate northward (toward and even beyond the equator) like the arms of a starfish. Where these radial rifts emanate from the ring of ridges, the ridges appear to have been pushed (presumably by the same radial compressive stresses that formed the ridges) into the openings of the rifts,§ much like fold-belts are pushed into the openings of aulacogens on earth (18).

To examine the origin of these terrains and the associated tectonic features, we neglect the curvature of the surface of Enceladus and conceive the original unfractured shell of Enceladus as an elastic half-space with uniform Young's modulus E and Poisson's ratio $\nu = 0.3$ (the elastic properties). We construe the thermal anomaly on the surface of Enceladus as a manifestation of a source of heat (Fig. 1) that is buried under the TST and drives the advection machine. We model the source of heat as a part of the shell that differs from the rest of the shell only in its temperature. Therefore, the source of heat and the surrounding material are of one piece and have the same elastic properties, but the temperature of the source of heat is higher than the temperature of the surrounding material by a prescribed temperature contrast ΔT. The source of heat has a flat upper surface and a flat bottom surface, both parallel to the surface of Enceladus; it is topped by a layer of uniform thickness that may be construed as the crust of the TST; and it tops a rocky core, which, for simplicity, we take to have the same elastic properties as the rest of Enceladus. For reasons explained later, we make the thickness of the source of heat and the thickness of the crust of the TST equal to the spacing between tiger stripes, 35 km. In plan view, we make the shape and orientation of the source of heat mirror the shape and orientation of both the TST and the thermal anomaly. As a first approximation, we disregard the slightly rectangular shape of the TST (and the thermal anomaly) and take the plan view of the source of heat to be a 175 $\times$ 175-km square with two sides parallel to an x axis oriented 45°W (Fig. 3*A*). (The results do not depend crucially on the geometry of the source of heat: they would be almost the same if we took the plan view of the source of heat to be a circle.)

The source of heat, with a coefficient of thermal expansion α, tends to expand driven by the temperature contrast ΔT. The thermal expansion of the source of heat is constrained by the surrounding material, leading to the development of stresses. To compute these stresses, we use the mathematical solution for a center of dilatation in an elastic half-space as a Green's function (20) (see *Appendix*). Fig. 3*C* shows the stresses σ_x and σ_y (see Fig. 3*B* for notation) that develop on the surface of Enceladus as a result of the constrained expansion of the source of heat.

At a distance of $\approx$100 km from the pole, the radial stresses (including σ_x along the x axis and σ_y along the y axis) vanish, and the hoop stresses (including σ_y along the x axis and σ_x along the y axis) take moderate tensile values (Fig. 3*C*). Thus, adjacent to the TST there is a relatively unstressed, narrow annular region that may show modest topography and no salient tectonic features, in accord with observations (Figs. 2 and 3*D*).

At farther distances from the pole, the radial stresses are compressive, and the hoop stresses are tensile (Fig. 3*C*). Driven by the compressive radial stresses (which peak at a distance of $\approx$140 km from the pole; Fig. 3*C*), a ring of ridges $\approx$280 km in diameter may form around the TST (Fig. 3*D*). Driven by both the tensile hoop stresses (which act as tearing agents) and the compressive radial stresses (which act as splitting agents), a set

GEOLOGY

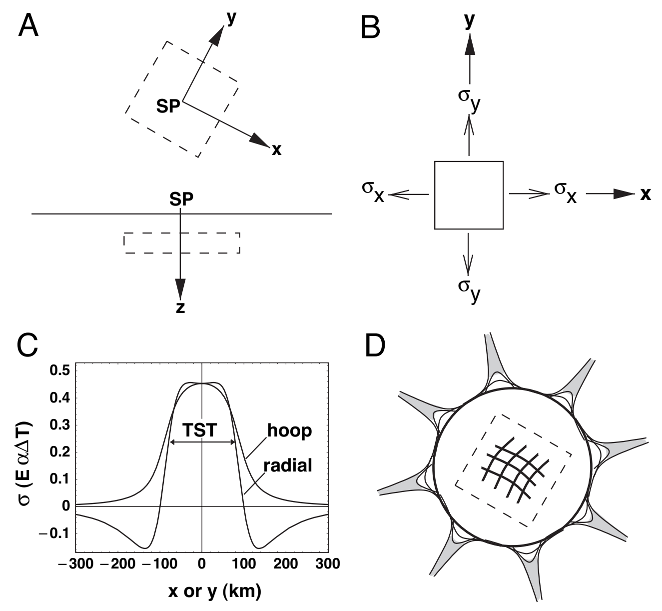

Fig. 3. Mechanical model explaining the formation of the tectonic features on the southern hemisphere. (*A*) Plan view and cross-section view of the mechanical model with a square TST. The pole is marked SP. (*B*) Stress element with stresses σ_x and σ_y. (*C*) Surface stresses along the *x* or *y* axis for the mechanical model with a square TST. (*D*) Tectonic features associated with the mechanical model with a square TST.

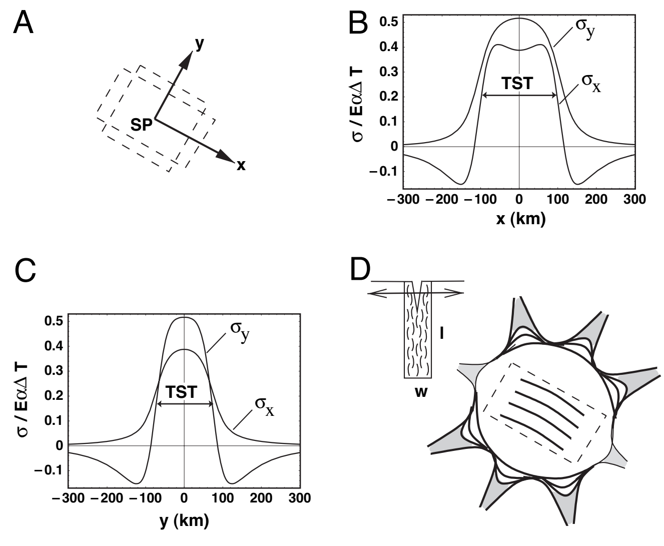

Fig. 4. Mechanical model explaining the formation of the tectonic features on the southern hemisphere, including the orientation of the tiger stripes. (*A*) Plan views of the mechanical model with a square TST and the mechanical model with a rectangular TST. The pole is marked SP. (*B*) Surface stresses along the *x* axis for the mechanical model with a rectangular TST. (*C*) Surface stresses along the *y* axis for the mechanical model with a rectangular TST. (*D*) Tectonic features associated with the mechanical model with a rectangular TST. (*Inset*) Cross-sectional slice of cracked material of thickness *w*.

of radial rifts may open up north of the ring of ridges (Fig. 3 *C* and *D*). Where one of these radial rifts opens up, a portion of the ring of ridges may be locally pushed into the rift (Figs. 2 and 3*D*), in accord with observations.

Because the radial rifts propagate for an indefinitely long distance in the radial direction, we reason that the distance between successive rifts along the ring of ridges must be set by *D*, the depth to which the radial rifts propagate. Now, the stresses decay with depth below the flat bottom surface of the source of heat, and the decay length is set by the thickness of the (expanding) source of heat. Thus, we can estimate $D \approx$ (thickness of the crust of the TST) + (thickness of the source of heat) + (decay length) $\approx 3 \cdot 35$ km = 105 km. The likely number of radial rifts is then $p/D \approx 8$, where p is the perimeter of the ring of ridges. (Note that this result is predicated upon our choice of a thickness of 35 km for both the crust and the source of heat.) The number of rifts in the interval from 180°W to 360°W is three (Fig. 2), and so to first order, our model is consistent with observations. The source of heat could be thicker than 35 km to account for the somewhat low number of rifts, or alternately, heterogeneity of the older terrains abutting the TST may control the fracture spacing to some degree.

On the TST, above the source of heat, σ_x and σ_y are both tensile (Fig. 3*C*). In fact, these stresses are tensile over the entire crust of the TST, but they change discontinuously from tensile to compressive at the interface between the constraining crust and the expanding source of heat. Driven by the tensile stresses, a set of parallel fractures, the tiger stripes, may cut vertically through the crust (Figs. 2 and 3*D*), up to a depth of 35 km. Then, the spacing between successive fractures will be approximately equal to the thickness of the crust, or ≈35 km, in accord with observations. [The relation spacing ≈ thickness holds close to the free surface of a fracturing layer bonded to a uniformly strained substrate, i.e., a substrate exhibiting no localized modes of deformation; the relation does not necessarily hold close to the bond between the fracturing layer and the substrate or when the fracturing layer is sandwiched between uniformly strained substrates (21, 22).] Note, however, that in this model σ_x is comparable to σ_y everywhere on the TST, and the tiger stripes may form parallel to either the *x* or the *y* axis (or any other radial axis).

To be able to predict the orientation of the tiger stripes, we change the in-plane dimensions of the source of heat to $(175 \cdot 1.2) \times (175/1.2)$ km (Fig. 4*A*), with the longer sides parallel to the *x* axis, so that in plan view the shape of the source of heat mirrors the shape of the TST (or the isotherm of 77 K) more faithfully than before. (We would obtain very similar results if we took the plan view of the source of heat to be an ellipse.) The distribution of stresses for the model with a rectangular TST (Fig. 4 *B* and *C*) is very similar to the distribution of stresses for the model with a square TST (Fig. 3*C*). Nevertheless, now $\sigma_y > \sigma_x$ everywhere on the TST, and the tiger stripes tend to form parallel to the longer sides of the TST, in accord with observations (Figs. 2 and 4). Further, after these tiger stripes form, σ_y must vanish in the crust of the TST, and the crust becomes less constrained in the direction of the shorter sides of the TST. To restore equilibrium, the stresses must intensify north of the longer sides of the TST. Thus, the ring of ridges may become especially prominent along the longer sides of TST, in accord with observations (Figs. 2 and 4*D*).

To estimate the temperature contrast required to form the tiger stripes, we write $\sigma_f = 0.5E\alpha\Delta T$, where σ_f is the tensile stress at failure and 0.5 is the maximum value of the tensile stress in units of $E\alpha\Delta T$ (from Fig. 4 *B* and *C*). The tensile strain at failure, σ_f/E may range from 0.1% to 0.01% and is roughly independent of the temperature (23–25); thus, using $\alpha = 5 \times 10^{-5}$/K, we compute ΔT = 4–40 K for a plausible lower bound on the temperature contrast.

In large masses of ice and other quasibrittle materials, a fracture does not form as a single cut through the material, but rather as a slice of finite width *w* (measured normal to the slice) where the material is criss-crossed by multiple subparallel cracks (26). As this slice of cracked material is torn apart, a few cracks may propagate and link up to form a single cut, whereas other cracks become arrested and close up. In the Arctic Ocean, for example, slices of cracked sea ice may have a width w of several kilometers and reach a length $l \approx 20$ km (Fig. 4*D Inset*) (25). Thus, we conceive a tiger stripe as a slice of cracked material that cuts vertically through 35 km of the crust of the TST. The width of this slice of cracked material is likely to increase with depth (Fig. 1); in fact, the slices of cracked material associated with successive tiger stripes may merge with one another at the bottom of the crust, where the crust must remain compatible with the spatially uniform deformation of the underlying source of heat. Close to the surface of the TST the width of a slice of cracked material is likely to be $w = 2$ km, the same width as the trough (of depth 0.5 km) that constitutes the surface expression of a tiger stripe (Fig. 1). Within a tiger stripe, in the associated slice of cracked material, some cracks may seal partially as a result of the refreezing of advected H_2O and gases, and others cracks grow in response to the explosive dissociation of clathrates and tectonic disturbances such as tidal deformation. At the same time, the slice of cracked material loses mass through the eruption of plumes, leading to the exhumation of a surficial trough with the same width as the slice of cracked material.

The plumes are but leaks in the advection machine of Enceladus. In fact, Kieffer *et al.* (7) estimate that the rate of discharge of the plumes [100–350 kg/sec (27)] constitutes only $\approx$10% of the total mass flux of the products of clathrate dissociation. If we assume that in the course of time the discharge of the plumes has led to the exhumation of four 130-km-long, 0.5-km-deep, 2-km-wide tiger-stripe troughs (Fig. 1), we can estimate a lower bound for the elapsed time of 50,000–170,000 years. Alternatively, if we assume that in the course of time the discharge of the plumes has led to the formation of a regional topographic depression of volume $\approx 1.3 \times 10^4$ km^3 (28), we can estimate an elapsed time of 1–4×10^6 years (28, 29). The remaining 90% of the total mass flux could refreeze near the surface (7, 10), giving up its heat content there and providing for the thermal anomaly and the hotspots documented by Spencer *et al.* (3).

In size, Enceladus is dwarfed by the other planets with active endogenic activity. The mechanism of the source of heat remains controversial, with tidal deformation and radioactive decay as major contenders (10, 30, 31). (Both these mechanisms are compatible with our model of Enceladus.) We have seen that a deep source of heat moderately hotter than the surrounding icy shell ($\Delta T \approx 4$–40 K, according to our estimate) is in itself sufficient to account for the observed surface morphology (which does not imply substantial deformation by creep), rate of heat transport (which is compatible with frigid temperatures), and plume eruption (which does not require the presence of liquids). A frigid, stiff, and thoroughly solid Enceladus may elicit fewer hopes of finding extraterrestrial life than a cold, creeping Enceladus with liquid water close to the surface, but it is consistent with observations, and perhaps more compatible with what might be surmised of a minuscule, icy moon.

Appendix: Surface Stress Calculation

To obtain the stresses on the surface (Figs. 3*C* and 4 *B* and *C*), we use the expressions for the in-plane displacements on the surface (x, y) associated with a differential source of heat of volume dV located at a depth c under the point $x = y = 0$ (4): $du_x = (1 + \nu)\alpha\Delta Tx/\pi dVR^{3/2}$ and $du_y = (1 + \nu)\alpha\Delta Ty/\pi dVR^{3/2}$, where $R = (x^2 + y^2 + c^2)^{3/2}$. The attendant strains on the surface follow as $d\varepsilon_x = \partial(du_x)/\partial x$ and $d\varepsilon_y = \partial(du_y)/\partial y$, and the attendant stresses on the surface as $d\sigma_x = E/(1 - \nu^2)(d\varepsilon_x + \nu d\varepsilon_y)$ and $d\sigma_y = E/(1 - \nu^2)(d\varepsilon_y + \nu\, d\varepsilon_x)$. Last, we compute the stresses on the surface associated with a source of heat of finite volume by integrating the expression for $d\sigma_x$ and $d\sigma_y$ (which play the role of Green's functions) over the volume of the source of heat.

We thank Bruce Jakosky and Johannes Weertman for insightful reviews.

1. Kargel JS (2006) *Science* 311:1389–1391.
2. Porco CC, Helfenstein P, Thomas PC, Ingersoll AP, Wisdom J, West R, Neukum G, Denk T, Wagner R, Roatsch T, *et al.* (2006) *Science* 311:1393–1401.
3. Spencer JR, Pearl JC, Segura M, Flasar FM, Mamoutkine A, Romani P, Buratti BJ, Hendrix AR, Spilker LJ, Lopes RMC (2006) *Science* 311:1401–1405.
4. Davies JH (2003) *J Appl Mech* 70:655–660.
5. Tian D, Stewart AIF, Toon OB, Larsen KM, Esposito LW (2007) *Icarus* 188:154–161.
6. Waite JH, Jr, Combi MR, Ip W-H, Cravens TE, McNutt, RL, Jr, Kasprzak W, Yelle R, Luhmann J, Niemann H, Gell D, *et al.* (2006) *Science* 311:1419–1422.
7. Kieffer SW, Lu X, Bethke CM, Spencer JR, Marshak S, Navrotsky A (2006) *Science* 314:1764–1766.
8. Fateev EG (2006) *Solar Syst Res* 40:400–411.
9. Bird RB, Stewart WE, Lightfoot EN (2002) *Transport Phenomena* (Wiley, New York), 2nd Ed, Table 14.1-1.
10. Nimmo F, Spencer JR, Pappalardo RT, Mullen ME (2007) *Nature* 447:289–291.
11. Lorenz RD (2002) *Icarus* 156:176–183.
12. Barr AC, Pappalardo RT (2005) *J Geophys Res* 110:E12005.
13. Barr AC, McKinnon WB (2007) *Geophys Res Lett* 34:L09202.
14. Durham WB, Kirby SH, Stern LA, Zhang W (2003) *J Geophys Res* 108:2182.
15. Greeley R, Chyba CF, Head JW, III, McCord TB, McKinnon WB, Pappalardo RT, Figueredo P (2004) in *Jupiter: The Planet, Satellites and Magnetosphere*, eds Bagenal F, Dowling TE, McKinnon WB (Cambridge Univ Press, Cambridge, UK), pp 329–362.
16. Pappalardo RT, Reynolds SJ, Greeley R (1997) *J Geophys Res* 102:13369–13380.
17. Nimmo F, Pappalardo RT (2006) *Nature* 441:614–616.
18. Marshak S (2004) *Memoir* 82:131–156.
19. Cassini Imaging Team (2007) *The Enceladus Atlas*. Available at: http://ciclops.org/maps.
20. Mindlin RD, Cheng DH (1950) *J Appl Phys* 21:931–933.
21. Bažant ZP, Ohtsubo H (1977) *Mech Res Commun* 4:353–366.
22. Ji S, Saruwatari K (1998) *J Struct Geol* 20:1495–1508.
23. Sloan ED, Jr (1997) *Clathrate Hydrates of Natural Gases* (Dekker, New York), 2nd Ed, Section 2.2, Table 2.7.
24. Schulson EM (1999) *J Minerals Metals Mater Soc* 51:21–27.
25. Bažant ZP (2002) *J Appl Mech* 69:11–18.
26. Bažant ZP (2004) *Proc Natl Acad Sci USA* 101:13400–13407.
27. Hansen CJ, Esposito L, Stewart AIF, Colwell J, Hendrix A, Pryor W, Shemansky D, West R (2006) *Science* 311:1422–1425.
28. Thomas PC, Burns JA, Helfenstein P, Squyres S, Veverka J, Porco C, Turtle EP, McEwen A, Denk T, Giese B, *et al.* (2007) *Icarus*, in press.
29. Matson DL, Castillo JC, Lunine J, Johnson TV (2007) *Icarus* 187:569–573.
30. Schubert G, Anderson JD, Travis BJ, Palguta J (2007) *Icarus* 188:345–355.
31. Meyer J, Wisdom J (2007) *Icarus* 188:535–539.